Ocean Modelling 28 (2009) 66–74

Contents lists available at ScienceDirect

Ocean Modelling

journal homepage: www.elsevier.com/locate/ocemod

Useful time-stepping methods for the Coriolis term in a shallow water model

Roy A. Walters [a,*], Emily M. Lane [b], Emmanuel Hanert [c]

[a] 6051 Hunt Road, Victoria, BC, Canada V8Y 3H7
[b] NIWA, P.O. Box 8602, Christchurch, New Zealand
[c] Department of Environmental Sciences and Land Planning, Université catholique de Louvain, Croix du Sud 2/16, B-1348 Louvain-la-Neuve, Belgium

ARTICLE INFO

Article history:
Received 4 February 2008
Received in revised form 18 October 2008
Accepted 21 October 2008
Available online 8 November 2008

Keywords:
Shallow water equations
Gravity waves
Coriolis
Time discretization
Stability

ABSTRACT

The attempt to simultaneously optimize stability, accuracy, and efficiency in an ocean model leads to a wide range of methods that are potentially useful. For some models, a major issue is the efficient integration of the Coriolis term when the underlying numerical model uses a semi-implicit time integration. Existing numerical models treat this integration with a variety of methods including explicit Adams–Bashforth schemes and implicit schemes. The semi-implicit approach is useful in that it provides a method to remove restrictive stability constraints and mode splitting errors. Published literature would suggest that many if not most standard explicit methods for the Coriolis term are unstable. On the other hand, implicit integration of the Coriolis term is very inefficient for staggered grid models with normal velocity degrees of freedom as it leads to inversion of a large, sparse velocity matrix. Our purpose is to explore and compare a variety of explicit or essentially explicit treatments of the Coriolis term. An analysis of the discretized shallow water equations indicates that some of the explicit methods are stable under somewhat relaxed conditions. Of these, the third-order Adams–Bashforth and the FBT scheme show good behavior. Numerical examples of coastal and deep ocean simulations illustrate the findings.

1. Introduction

One goal in the development of an ocean model is to optimize stability, accuracy, and efficiency simultaneously. Many choices in spatial and temporal discretization, solvers, and other technical details are available. However, in practical terms only a subjective balance between these goals is readily attainable and this balance in many cases depends on the specific problem under consideration.

Nonetheless, some of these choices such as removing stability constraints (Dukowicz and Smith, 1994; Casulli and Cattani, 1994; Kwok, 1996) are advantageous for a wide range of problems. Other choices such as forming a discrete wave equation from a combination of the free surface equation and momentum equations enhances efficiency by reducing matrix size (Walters and Casulli, 1998; Casulli and Walters, 2000). On the other hand, using higher-order methods tends to impact efficiency while improving accuracy (Barragy and Walters, 1998) and may or may not be useful. Here, the focus is on an attempt to optimize the balance between stability, accuracy, and efficiency in the numerical treatment of the Coriolis term in a shallow water model.

Implicit methods can remove restrictive stability constraints and have the added advantage of removing mode splitting errors when a different time step is used for the barotropic and baroclinic modes (Dukowicz and Smith, 1994). Many of the older global ocean models and derivatives of them that originally used a rigid lid approximation now have a free surface option. For the most part, the free surface approximation follows the methods described in Dukowicz and Smith (1994) where the free surface equation is advanced in time with a backward Euler scheme and the momentum equations are approximated with a Leap Frog (LF) scheme. This approach is appropriate for problems where the fast gravity waves are not of interest and must be damped.

The particular class of models of interest here are regional scale models where tides, atmospheric exchanges, and coastal runoff are major forcings, and coastal geometry and topography are important. The features of interest include tsunami, infragravity waves, tides, and longer period transient effects. For this class of problems, a backward Euler scheme leads to excessive damping and a centered scheme is more accurate. Here, we consider semi-implicit methods where some terms are integrated implicitly using the θ-method and other terms are integrated explicitly.

The semi-implicit approach was chosen because it removes the major stability constraints on gravity waves and the vertical component of viscous stresses. In addition, this approximation eliminates the computational modes present with the LF treatment of the momentum equations and removes mode splitting errors by using the same time step for the barotropic and baroclinic modes. However, the spatial discretization of the Coriolis term results in a large, sparse, skew-symmetric matrix. Hence, a semi-implicit treatment of the Coriolis term usually requires the solution of a large matrix for

* Corresponding author. Tel.: +1 250 652 8995.
E-mail addresses: rawalters@shaw.ca (R.A. Walters), e.lane@niwa.co.nz (E.M. Lane), emmanuel.hanert@uclouvain.be (E. Hanert).

1463-5003/$ - see front matter © 2008 Elsevier Ltd. All rights reserved.
doi:10.1016/j.ocemod.2008.10.004

the three-dimensional velocity (Danilov et al., 2004). This approach is not practical for our approach as it leads to a very inefficient model. Ideally, the Coriolis term can be integrated by stable explicit methods or essentially explicit methods which would be more efficient in this case. Essentially explicit defines those methods such as split step that can be reduced to an explicit scheme.

Unfortunately, many explicit methods are unconditionally unstable. A simple forward Euler (fE) integration of the equation for inertial oscillations is unconditionally unstable. Durran (1991) shows that the third-order Adams–Bashforth method (AB3) is stable for the same equations, but is unconditionally unstable for a two-frequency system where the fast oscillation (gravity waves) is treated semi-implicitly. An important point here is that the simplified oscillation equations do not give a complete picture of stability and the complete shallow water equations must be analyzed. Hence we have examined the semi-implicit treatment of the shallow water equations in this study.

Of course, choices for the discretization of the Coriolis term have been considered in all existing ocean models. For example, a generalized Forward–Backward scheme is described for ROMS (Shchepetkin and McWilliams, 2005; Kanarska et al., 2007) where the Coriolis term may be approximated with AB3. In addition, MITgcm is an ocean model that follows the approach of Marshall et al. (1997) with a backward Euler time integration and uses a modified second-order Adams–Bashforth method (AB2) for the Coriolis term. AB2 is unstable for the inviscid case. However, modifying the coefficients provides a stable method although formal accuracy deteriorates (Marshall et al., 1997).

The two models that bear the closest resemblance to the model we are considering, RiCOM (Walters and Casulli, 1998), are UNTRIM (Casulli and Zanolli, 2002) and SUNTANS (Fringer et al., 2006). UNTRIM is an unstructured grid model with semi-implicit time integration that uses a split step integration of the Coriolis term (Casulli and Walters, 2000). SUNTANS has a similar discretization but uses the second-order Adams–Bashforth method (AB2) (Fringer et al., 2006).

Thus, a number of methods for treating the Coriolis term have been utilized in various ocean models. However, there appears to be a lack of analysis that compares these methods for stability, accuracy, and efficiency. This is particularly true for the case of semi-implicit time integration, except for work by Kwok (1996) who examines a forward Euler treatment. Hence, we have analyzed the amplification (stability) characteristics of the shallow water equations (SWE) for a number of treatments of the Coriolis term. We consider a semi-implicit approximation of the linearized SWE rather than the simplified equations for inertial oscillations such as Durran (1991) considered. A more complete treatment of the problem is expected to lead to better perspective of useful and efficient methods.

In the next section, the governing equations (shallow water equations) are defined along with the analysis methods. We consider the equations to be continuous in space for generality. Hence, the discrete spatial operators must be added to describe a particular scheme (see for instance, LeRoux et al. (2007) for an analysis of a variety of discretization schemes). Although the explicit methods are applicable to a wide range of discretizations, some are more useful with staggered grids with normal velocity degrees of freedom and others can only be applied to grids that use full vectors. This point is discussed along with the particular methods.

In the following section, several explicit time integration schemes are examined including forward Euler (fE) which is generally known to be unstable, second-order Adams–Bashforth (AB2) which Marshall indicates is unstable for the inviscid equations, and third-order Adams–Bashforth (AB3). In addition, we consider the Forward–Backward in Time (FBT) scheme. Finally, we give some numerical examples and conclusions.

2. Formulation

2.1. Shallow water equations

The basic equations considered here are the two-dimensional shallow water equations. These equations are derived by vertically integrating the Reynolds-averaged Navier–Stokes equations and using the hydrostatic assumption and the Boussinesq approximation (Pinder and Gray, 1977). The continuity equation (free surface equation) is

$$\frac{\partial \eta}{\partial t} + \nabla \cdot (H\mathbf{u}) = 0 \tag{1}$$

and the momentum equation expressed in nonconservative form is

$$\frac{d\mathbf{u}}{dt} + f\hat{\mathbf{z}} \times \mathbf{u} + g\nabla\eta + \frac{\tau_b}{\rho H} = 0 \tag{2}$$

where the coordinate directions (x,y,z) are aligned in the east, north, and vertical directions; $\mathbf{u}(x,y,t)$ is the depth-averaged horizontal velocity with components (u,v); f is the Coriolis parameter; $\hat{\mathbf{z}}$ is the upward unit vector; $h(x,y)$ is the water depth measured from a reference elevation; $\eta(x,y,t)$ is the distance from the reference elevation to the free surface; $H(x,y,t)$ is the total water depth, $H = \eta - h$; g is the gravitational acceleration; ρ is a reference density; and ∇ is the horizontal gradient operator $(\partial/\partial x, \partial/\partial y)$. The bottom stress $\boldsymbol{\tau}_b$ is given by

$$\frac{\boldsymbol{\tau}_b}{\rho} = C_D \mid \mathbf{u} \mid \mathbf{u} = \gamma H\mathbf{u} \qquad (z = h), \tag{3}$$

where C_D is a bottom drag coefficient, and γ is defined by this equation. For the test problems, essential boundary conditions on η are set at open boundaries, and $(\mathbf{u} \cdot \hat{\mathbf{n}}) = 0$ (no normal flow, where $\hat{\mathbf{n}}$ is the unit normal) is set on land boundaries.

2.2. Time discretization

The central issue is how to integrate the Coriolis term with explicit methods and the gravity wave terms with semi-implicit methods in such a way as to ensure a stable, accurate, and efficient solution. For the semi-implicit time integration, we use the θ-scheme where a variable ϕ is approximated as $\phi^{n+\theta} = \theta\phi^{n+1} + (1-\theta)\phi^n$.

For this analysis, we use the linearized shallow water equations; *i.e.,* depth is taken to be constant in the continuity equation, advection is neglected, and γ is a constant in the momentum equation. The resulting semi-implicit time discretization of the continuity (free surface) and momentum equations is

$$\frac{\eta^{n+1} - \eta^n}{\Delta t} = -\nabla \cdot [\theta H\mathbf{u}^{n+1} + (1-\theta)H\mathbf{u}^n] \tag{4}$$

$$\frac{\mathbf{u}^{n+1} - \mathbf{u}^n}{\Delta t} + \gamma\mathbf{u}^{n+1} = -g\nabla[\theta\eta^{n+1} + (1-\theta)\eta^n] + \mathbf{F}(\mathbf{u}) \tag{5}$$

where $\mathbf{F}(\mathbf{u})$ represents the treatment of the Coriolis term which is defined in the next sections.

Linearized equations are necessary in order to find analytical expressions for the complex amplification factors in the next section. However, in the results section we use the full nonlinear model to evaluate efficiency, accuracy, and stability.

3. Stability and accuracy

An analysis of the discretized equations can proceed in several ways. One approach is to use amplification factors which give the complex admittance per time step (Mesinger and Arakawa, 1976). Another is to use propagation factors which give the amplitude and phase errors per wavelength (Leendertse, 1967). Yet

another is to use a classical Fourier analysis which gives the dispersion relation as well as damping factors and phase speed (Dukowicz and Smith, 1994). Since we are concerned with stability issues, the former provides a more convenient analysis method.

The complex amplification factors are calculated using standard methods (Mesinger and Arakawa, 1976; Durran, 1991). First the amplification factor is defined as $\phi^{n+1} = A\phi^n$ where A is the complex amplification factor, ϕ is one of the dependent variables, and n denotes the time level. This relation is applied to the governing equations (sometimes repeatedly) in order to reduce the dependent variables to the same time level. Then, the determinant of the coefficient matrix is solved for A. As may be seen, the real difficulty is solving an Nth order polynomial for A.

3.1. Semi-implicit gravity wave terms

As a baseline, first consider the gravity wave problem without Coriolis. Using a semi-implicit approach, the gravity wave terms are evaluated in the time interval $[t^{n+1},t^n]$ at the time $t^n + \theta\Delta t$. The linear shallow water equations can be written

$$\eta^{n+1} - \eta^n = -\Delta t\nabla\cdot[\theta H\mathbf{u}^{n+1} + (1-\theta)H\mathbf{u}^n] \tag{6}$$

$$\mathbf{u}^{n+1} - \mathbf{u}^n + \gamma\Delta t\mathbf{u}^{n+1} = -g\Delta t\nabla[\theta\eta^{n+1} + (1-\theta)\eta^n]. \tag{7}$$

We consider the case where η and $\mathbf{u}$ are continuous in space and expand them according to $\phi = \phi_k e^{i\mathbf{k}\cdot\mathbf{x}}$ where the wave-number $\mathbf{k} = (k_x,k_y)$ and $k = |\mathbf{k}|$. Dropping the subscript k because the equations are linear, the equations then become

$$(A-1)\eta = -i\Delta tH(\theta A + (1-\theta))\mathbf{k}\cdot\mathbf{u}, \tag{8}$$

$$(A(1+\gamma\Delta t) - 1)\mathbf{u} = -ig\Delta t(\theta A + (1-\theta))\mathbf{k}\eta. \tag{9}$$

By substituting (9) into (8) we get for $\gamma = 0$

$$((1+E\theta^2)A^2 - 2A(1-E\theta(1-\theta)) + 1 + E(1-\theta)^2)\eta = 0, \tag{10}$$

where $E = gH\Delta t^2k^2 = (ck\Delta t)^2$, $c = \sqrt{gH}$ being the phase speed. Thus the roots of A are

$$A = \frac{1 - E\theta(1-\theta) \pm i\sqrt{E}}{1+E\theta^2}. \tag{11}$$

The amplitude of A is

$$A = \frac{\sqrt{1 + E(1-2\theta(1-\theta)) + E^2\theta^2(1-\theta)^2}}{1+E\theta^2} \tag{12}$$

which is equal to one for $\theta = 0.5$ and less than one for $\theta > 0.5$; *i.e.*, the equations are unconditionally stable for $\theta \geqslant 0.5$. For $\theta < 0.5$, the CFL stability limit applies.

The amplification factor of the exact solution is $A_e = e^{ick\ \Delta t}$. The relative phase error is thus

$$R = \frac{\arg A}{\arg A_e} = \frac{1}{ck\Delta t}\arctan\left(\frac{\Im[A]}{\Re[A]}\right). \tag{13}$$

In this case R becomes

$$R = \frac{1}{ck\Delta t}\arctan\left(\frac{ck\Delta t}{1-(ck\Delta t)^2(1-2\theta(1-\theta))}\right). \tag{14}$$

The term $ck\Delta t$ can be written as $C_w(k\Delta e)$ where C_w is the wave Courant number (CFL parameter) defined by $C_w = c\Delta t/\Delta e$ and Δe is a length scale that is related to an element edge length. Hence the horizontal axis of Fig. 1 can be written in terms of $(k\Delta e)$ (with C_w as a scaling parameter) and thus directly compared to a variety of results from dispersion analysis; *e.g.*, LeRoux et al. (2007). For a spatially discretized treatment, the grid cutoff is $(k\Delta e) = \pi$. Then for large C_w the damping extends to lower wavenumber as is well known. From this, we may observe that the damping in the figure

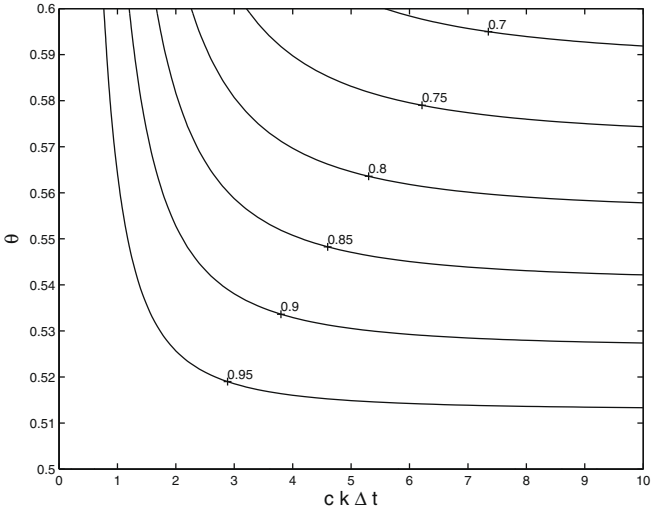

Fig. 1. Contour plot of the magnitude of the amplification factor $|A|$ for gravity waves as a function of θ and $ck\Delta\ t$ for $\Delta t = 360$ s.

is dominated by the semi-implicit treatment in time and the value of θ. However, these effects are primarily felt at large wavenumber (toward the grid cutoff) and diminish toward low wavenumber (well resolved motions). As a result, the solution at low wavenumber is more accurate and the effects of damping also diminish. While the value for θ determines the damping, the next subsections show that the explicit method used for the Coriolis term controls the stability limit at the bottom of the figure where $A = 1$.

3.2. Semi-implicit gravity wave terms with explicit (fE) Coriolis

The forward Euler (fE) treatment of the Coriolis term is unstable. However, this approximation is still used in some coastal ocean models where friction is used to stabilize the solution (Zhang and Baptista, 2008). This scheme is analyzed here for two reasons: it provides a simple case for understanding the methodology we use, and it provides a basis to assess the limits on the use of this scheme.

The semi-implicit form of the shallow water equations with explicit *i.e.*, forward Euler, treatment of the Coriolis term is

$$\eta^{n+1} - \eta^n = -\Delta t\nabla\cdot[\theta H\mathbf{u}^{n+1} + (1-\theta)H\mathbf{u}^n] \tag{15}$$

$$\mathbf{u}^{n+1} - \mathbf{u}^n = -g\Delta t\nabla[\theta\eta^{n+1} + (1-\theta)\eta^n] - f\hat{\mathbf{z}}\times\mathbf{u}^n. \tag{16}$$

Again, we may expand this in terms of wave-number $\mathbf{k}$, and we will also express the Coriolis term in matrix form. The continuity equation is unchanged from (8), however the momentum equation becomes

$$(A-1)\mathbf{u} = -ig\Delta t(\theta A + (1-\theta))\mathbf{k}\eta - \Delta tf\begin{pmatrix}0 & -1\\ 1 & 0\end{pmatrix}\mathbf{u}. \tag{17}$$

Rearranging for $\mathbf{u}$ gives

$$\begin{pmatrix}A-1 & -\Delta tf\\ \Delta tf & A-1\end{pmatrix}\mathbf{u} = -ig\Delta t(\theta A + (1-\theta))\mathbf{k}\eta, \tag{18}$$

i.e.,

$$\mathbf{u} = \frac{1}{(A-1)^2 + \Delta t^2f^2}\begin{pmatrix}A-1 & \Delta tf\\ -\Delta tf & A-1\end{pmatrix}[-ig\Delta t(\theta A + (1-\theta))\mathbf{k}\eta]. \tag{19}$$

As in the case of the semi-implicit gravity wave we may substitute this into (8). Noting that

$$\mathbf{k}\cdot\begin{pmatrix} A-1 & \Delta tf \\ -\Delta tf & A-1 \end{pmatrix}\mathbf{k} = (A-1)k^2$$

we get the following expression for A,

$$(A-1)((1+E\theta^2)A^2 - 2A(1-E\theta(1-\theta)) + 1 + E(1-\theta)^2 + \Delta t^2 f^2) = 0. \tag{20}$$

There are three roots to this equation. The real root $A = 1$ is the geostrophic mode and it would correspond to the slow Rossby mode on a β-plane approximation (LeRoux et al., 2007). The other two roots are complex conjugates and correspond to the Poincaré wave solution. They are

$$A = \frac{1 - E\theta(1-\theta) \pm i\sqrt{E + (1+E\theta^2)\Delta t^2 f^2}}{(1+E\theta^2)}. \tag{21}$$

Note that for $f = 0$ this collapses down to (11), the expression for gravity waves. For $\theta = 0.5$, $|A|^2 = 1 + \Delta t^2 f^2$ regardless of the value of E and thus the equation is unstable. For larger values of θ this situation changes and for

$$|f| \leqslant ck\sqrt{2\theta - 1}, \tag{22}$$

$|A| \leqslant 1$ and thus the equations are stable. Note that the spatially invariant mode corresponding to $k = 0$ will always be unstable as (22) will not hold for non-zero f.

Fig. 2 shows a contour plot of the magnitude of A as a function of θ and $ck\Delta t$ for $f = 1 \times 10^{-4}\ s^{-1}$ and $\Delta t = 360$ s. For $\theta > 0.5$ and $ck\Delta t$ large enough the amplification factor is less than one. Fig. 3 shows the contour $|A| = 1$ for different values of f. As f increases, the area where the scheme is unstable increases. The scheme is always unstable for $\theta = 0.5$ and for $ck\Delta t = 0$.

We may observe again that the damping in the figure is dominated by the semi-implicit treatment in time and the value of θ. However, these effects are primarily felt at large wavenumber (toward the grid cutoff) and diminish toward low wavenumber (well resolved motions). While the value for θ determines the damping, the explicit method used for the Coriolis term controls the stability limit at the bottom of the figure. For this case, the method is unstable for any value of θ with an arbitrary value of k.

The equations can be stabilized by sufficient friction as can be seen by deriving (20) using a positive finite value for γ. Nonetheless, this presents a serious problem in places where the velocity is zero and in the deep ocean where friction is small.

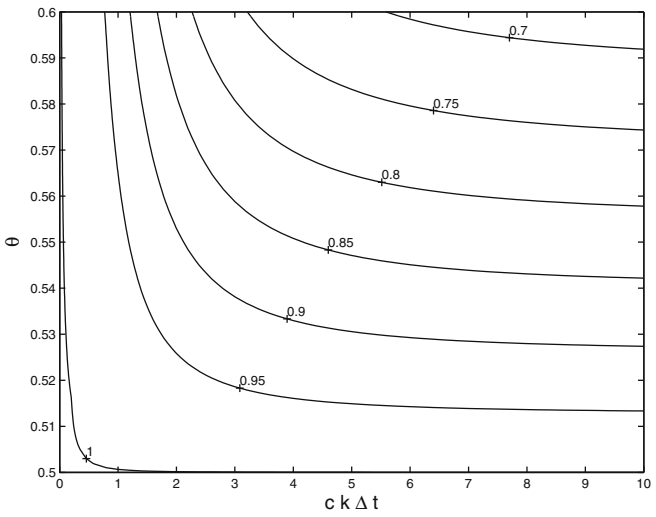

Fig. 2. Contour plot of the magnitude of the amplification factor $|A|$ for forward Euler as a function of θ and $ck\Delta t$ for $f = 1 \times 10^{-4}\ s^{-1}$ and $\Delta t = 360$ s.

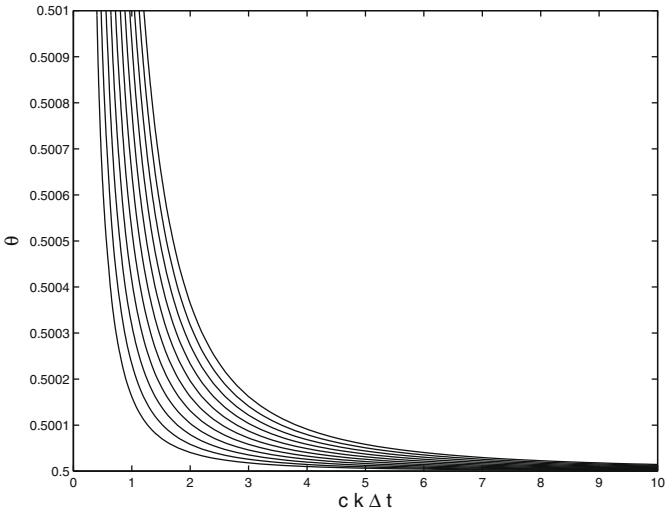

Fig. 3. Contour lines for $|A| = 1$ for forward Euler for $f = 5 \times 10^{-5}\ s^{-1}$ (lowest) to $f = 1.5 \times 10^{-4}\ s^{-1}$ (highest), $\Delta t = 360$ s.

3.3. Semi-implicit gravity wave terms with explicit (AB2) Coriolis

The semi-implicit form of the shallow water equations with second-order Adams–Bashforth treatment of the Coriolis term is

$$\eta^{n+1} - \eta^n = -\Delta t\nabla\cdot[\theta H\mathbf{u}^{n+1} + (1-\theta)H\mathbf{u}^n], \tag{23}$$

$$\mathbf{u}^{n+1} - \mathbf{u}^n = -g\Delta t\nabla[\theta\eta^{n+1} + (1-\theta)\eta^n] - f\hat{\mathbf{z}}\times\left(c_1 + \frac{c_2}{A}\right)\mathbf{u}^n, \tag{24}$$

where for second-order Adams–Bashforth, $c_1 = 3/2$ and $c_2 = -1/2$. Again, the continuity equation is unchanged from (8). Note that (24) is the same as (17) with f replaced by $f(c_1 + c_2/A)$. Thus we may use the same method to find the equation for A,

$$A^4(1+E\theta^2) - 2A^3(1 - E\theta(1-\theta)) + A^2(1 + E(1-\theta)^2 + \Delta t^2 f^2 c_1^2) + 2Ac_1c_2\Delta t^2 f^2 + c_2^2\Delta t^2 f^2 = 0. \tag{25}$$

In general, there are two complex values and their complex conjugates as roots of this equation. One of these roots is the physical mode shown here and the other root is a computational mode which has small amplitude.

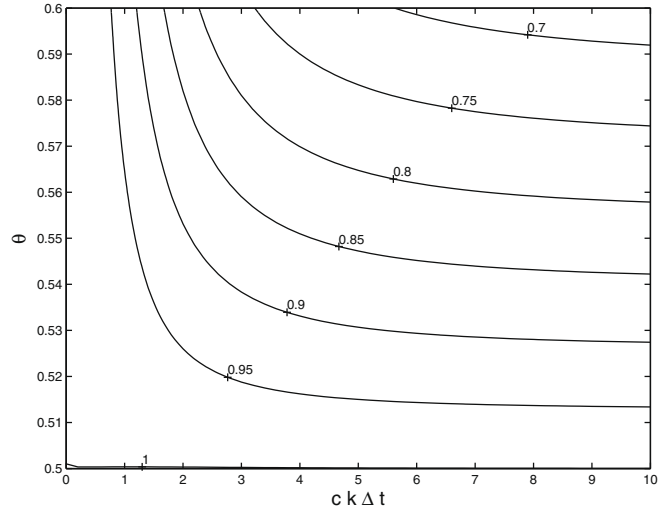

Fig. 4. Contour plot of the magnitude of the amplification factor $|A|$ for second-order Adams–Bashforth as a function of θ and $ck\Delta t$ for $f = 1 \times 10^{-4}\ s^{-1}$ and $\Delta t = 360$ s.

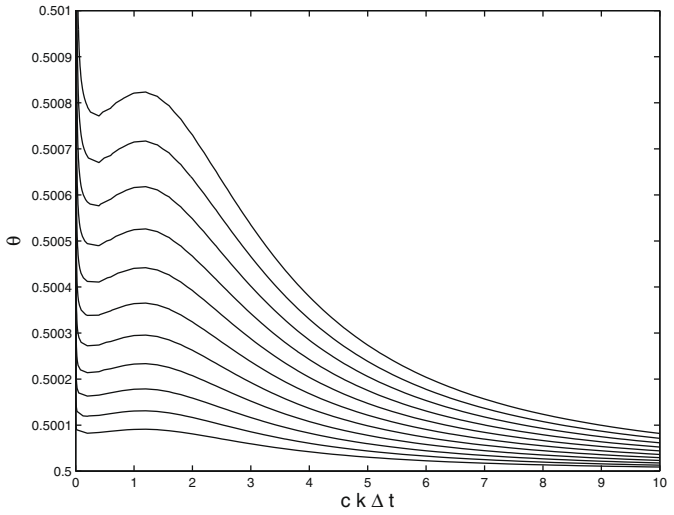

Fig. 5. Contour lines for $|A| = 1$ for second-order Adams–Bashforth for $f = 5 \times 10^{-5}\ s^{-1}$ (lowest) to $f = 1.5 \times 10^{-4}\ s^{-1}$ (highest), $\Delta t = 360$ s.

Although the stability limit is greatly reduced from the fE scheme, Figs. 4 and 5 show that AB2 is still unstable for $\theta = 0.5$ and for $k = 0$. Like the fE scheme, AB2 is slightly unstable for small values of k. Introducing damping by increasing θ is ineffective at small wavenumber. Like the fE scheme, AB2 can be stabilized by introducing friction. However, this option is not recommended for the same reasons as stated earlier.

Another option is to modify the weights such as suggested by Marshall et al. (1997). The weights are adjusted as $c_1 = 3/2 + \epsilon$ and $c_2 = -1/2 - \epsilon$ which effectively approximates the Coriolis term at time $n + 1/2 + \epsilon$. Marshall et al. (1997) suggests a value $\epsilon = 0.1$ The stability limit for this modified form is shown in Fig. 6. As may be seen, the scheme is now stable at $k = 0$ and the remaining stability constraint is rather weak, $\theta \geqslant 0.501$ approximately.

3.4. Semi-implicit gravity wave terms with explicit (AB3) Coriolis

The semi-implicit form of the shallow water equations with third-order Adams–Bashforth treatment of the Coriolis term is

$$\eta^{n+1} - \eta^n = -\Delta t \nabla \cdot [\theta H \mathbf{u}^{n+1} + (1-\theta) H \mathbf{u}^n], \tag{26}$$

$$\mathbf{u}^{n+1} - \mathbf{u}^n = -g\Delta t \nabla [\theta \eta^{n+1} + (1-\theta)\eta^n] - f\hat{\mathbf{z}} \times \left(c_1 + \frac{c_2}{A} + \frac{c_3}{A^2}\right)\mathbf{u}^n, \tag{27}$$

where for third-order Adams–Bashforth, $c_1 = 23/12$, $c_2 = -16/12$ and $c_3 = 5/12$. Again, the continuity equation is unchanged from (8). Eq. (27) is the same as (17) with f replaced by $f(c_1 + c_2/A + c_3/A^2)$. Using the same method to find the equation for A,

$$\begin{aligned} &A^6(1+E\theta^2) - 2A^5(1 - E\theta(1-\theta)) + A^4(1 + E(1-\theta)^2 + \Delta t^2 f^2 c_1^2) \\ &\quad + 2A^3 c_1 c_2 \Delta t^2 f^2 + A^2(2c_1c_3 + c_2^2)\Delta t^2 f^2 + 2Ac_2c_3\Delta t^2 f^2 \\ &\quad + c_3^2 \Delta t^2 f^2 = 0. \end{aligned} \tag{28}$$

Note that although this is a real polynomial, generally it has 3 complex values and their complex conjugates as roots. One of these roots is the physical mode shown here and the other two roots are computational modes which have small amplitude.

Fig. 7 shows a contour plot of the magnitude of A as a function of θ and $ck\Delta t$ for $f = 1 \times 10^{-4}\ s^{-1}$ and $\Delta t = 360$ s for the third-order Adams–Bashforth. Although the scheme is unstable for $\theta = 0.5$ for $ck\Delta t$ greater than 2, the area where A is greater than one is strongly confined to the axis. For $\theta > 0.501$ A is less than one for the range of f values considered here. Note that, like the forward Euler, the solution is damped quite strongly for larger values of θ. Fig. 8 shows the contour $|A| = 1$ for different values of f. As f increases, the area where the scheme is unstable increases but it is still a small area being confined to $\theta < 0.501$. The scheme is always unstable for $\theta = 0.5$ and $ck\Delta t > \approx 1.8$.

In general, AB3 represents a workable choice for an explicit approximation. The scheme has a rather minor stability constraint while it retains third-order accuracy. Moreover, it is an explicit scheme which allows the full efficiency of a particular numerical model to be realized.

3.5. Semi-implicit gravity wave terms with explicit (FBT) Coriolis

The Forward–Backward in Time (FBT) scheme tries to mimic a semi-implicit scheme by alternatively changing the order in which the two momentum equations are solved. The Coriolis term is always discretized by using the most recently computed velocity component. The FBT scheme was first mentioned by Sielecki (1968) and latter analyzed and improved by Beckers and Dele-

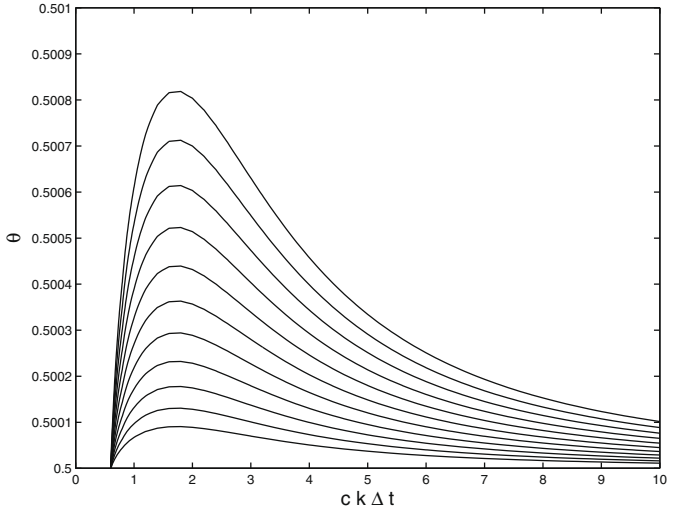

Fig. 6. Contour lines for $|A| = 1$ for modified second-order Adams–Bashforth for $f = 5 \times 10^{-5}\ s^{-1}$ (lowest) to $f = 1.5 \times 10^{-4}\ s^{-1}$ (highest), $\Delta t = 360$ s, $\epsilon = 0.1$.

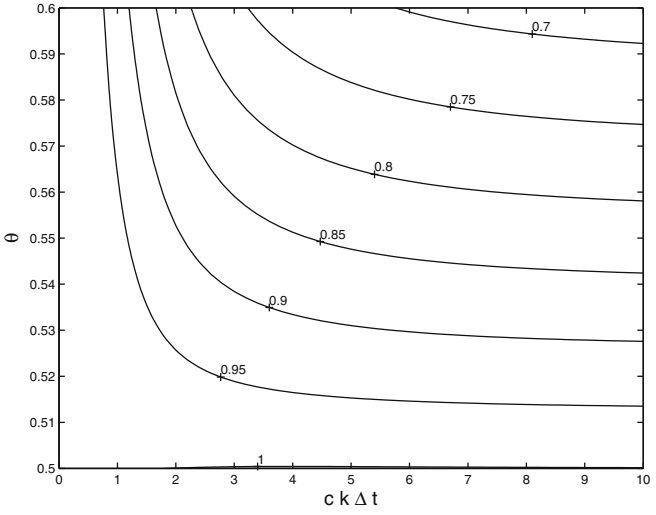

Fig. 7. Contour plot of the magnitude of the amplification factor $|A|$ for third-order Adams–Bashforth as a function of θ and $ck\Delta t$ for $f = 1 \times 10^{-4}\ s^{-1}$ and $\Delta t = 360$ s.

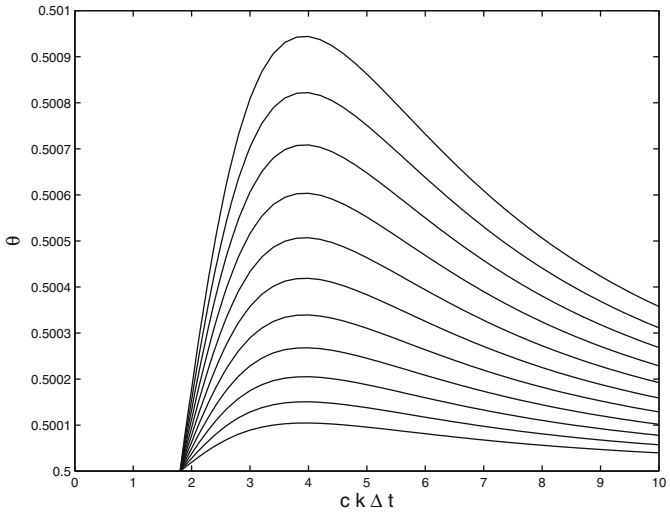

Fig. 8. Contour lines for $|A| = 1$ for third-order Adams–Bashforth for $f = 5 \times 10^{-5}\ s^{-1}$ (lowest) to $f = 1.5 \times 10^{-4}\ s^{-1}$ (highest), $\Delta t = 360$ s.

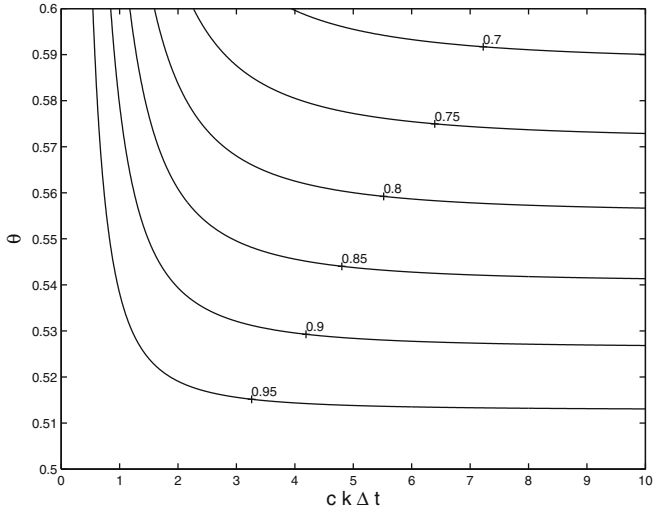

Fig. 9. Contour plot of the magnitude of the amplification factor $|A|$ for the FBT scheme as a function of θ and $ck\Delta\ t$ for $f = 1 \times 10^{-4}\ s^{-1}$ and $\Delta t = 360$ s.

ersnijder (1993). Here, a semi-implicit time integration scheme is used for the gravity wave terms and the Coriolis term is discretized with a FBT scheme. The time discretization is:

$$\eta^{n+1} = \eta^n - H\Delta t\nabla\cdot[\theta\mathbf{u}^{n+1} + (1-\theta)\mathbf{u}^n] \tag{29}$$

$$u^{n+1} = u^n + f\Delta t v^n - g\Delta t\frac{\partial}{\partial x}[\theta\eta^{n+1} + (1-\theta)\eta^n] \tag{30}$$

$$v^{n+1} = v^n - f\Delta t u^{n+1} - g\Delta t\frac{\partial}{\partial y}[\theta\eta^{n+1} + (1-\theta)\eta^n] \tag{31}$$

and

$$\eta^{n+2} = \eta^{n+1} - H\Delta t\nabla\cdot[\theta\mathbf{u}^{n+2} + (1-\theta)\mathbf{u}^{n+1}] \tag{32}$$

$$v^{n+2} = v^{n+1} - f\Delta t u^{n+1} - g\Delta t\frac{\partial}{\partial y}[\theta\eta^{n+2} + (1-\theta)\eta^{n+1}] \tag{33}$$

$$u^{n+2} = u^{n+1} + f\Delta t v^{n+2} - g\Delta t\frac{\partial}{\partial x}[\theta\eta^{n+2} + (1-\theta)\eta^{n+1}] \tag{34}$$

It can be seen that for each set of equations, the Coriolis term is first discretized explicitly and then implicitly. The order of the two momentum equations is switched in the second set of equations. As a result, the time discretization of the Coriolis term appears to be semi-implicit "on average". It has been shown that such a discretization prevents the Coriolis force from creating energy (Sielecki, 1968; Beckers and Deleersnijder, 1993).

To analyse the stability of this scheme, we compute the amplification factor for both sets of equations separately and then derive the amplification factor A defined over two time steps: $A^2 = A_1A_2$, where A_1 and A_2 are the propagation factors associated with Eqs. (29)–(34), respectively. Expanding η^n and $\mathbf{u}^n$ as before, Eqs. (29)–(31) then reduce to:

$$(A_1 - 1)\eta^n = -iH\Delta t(\theta A_1 + (1-\theta))\mathbf{k}\cdot\mathbf{u}^n, \tag{35}$$

$$(A_1 - 1)u^n = f\Delta t v^n - ig\Delta t(\theta A_1 + (1-\theta))k_x\eta^n, \tag{36}$$

$$(A_1 - 1)v^n = -f\Delta t A_1 u^n - ig\Delta t(\theta A_1 + (1-\theta))k_y\eta^n, \tag{37}$$

and Eqs. (32)–(34) can be recast as:

$$(A_2 - 1)\eta^{n+1} = -iH\Delta t(\theta A_2 + (1-\theta))\mathbf{k}\cdot\mathbf{u}^{n+1}, \tag{38}$$

$$(A_2 - 1)u^{n+1} = f\Delta t A_2 v^{n+1} - ig\Delta t(\theta A_2 + (1-\theta))k_x\eta^{n+1}, \tag{39}$$

$$(A_2 - 1)v^{n+1} = -f\Delta t u^{n+1} - ig\Delta t(\theta A_2 + (1-\theta))k_y\eta^{n+1}. \tag{40}$$

By using Eqs. (36,37), we can express $\mathbf{u}^n$ in terms of η^n in Eq. (35) and obtain the following equation for A_1:

$$(A_1 - 1) = -\frac{gH\Delta t^2(\theta A_1 + (1-\theta))^2}{(A_1-1)^2 + f^2\Delta t^2 A_1}(k_x^2 + k_y^2 - k_xk_yf\Delta t)(A_1 - 1). \tag{41}$$

By doing the same for A_2, we obtain:

$$(A_2 - 1) = -\frac{gH\Delta t^2(\theta A_2 + (1-\theta))^2}{(A_2-1)^2 + f^2\Delta t^2 A_2}(k_x^2 + k_y^2 + k_xk_yf\Delta t)(A_2 - 1). \tag{42}$$

Eqs. (41) and (42) are quadratic equations that can be solved for A_1 and A_2. Fig. 9 shows the absolute value of $A = \sqrt{A_1A_2}$ in terms of $ck\Delta t$ and θ. In that example, $f = 1 \times 10^{-4}\ s^{-1}$ and $\Delta t = 360$ s. The amplification factor is less or equal to one for all values of $ck\Delta t$ as long as $\theta \geqslant 0.5$.

The advantage of FBT over the AB3 is that it introduces no stability constraints while maintaining approximately the same accuracy for the amplification factor. However, FBT cannot be used with all types of discretization schemes. For approximations with 2 degrees of freedom (u,v) at each velocity node, FBT can be implemented in the same manner as shown here. Examples are the linear $(P_1 - P_1)$ finite element and the linear non-conforming finite element $(P_1^{NC} - P_1)$ (see LeRoux et al., 2007). On the other hand, FBT cannot be applied when there is only one degree of freedom at velocity nodes. An example is the Raviart–Thomas finite element of lowest-order (RT_0) which has the normal component of velocity defined on each edge and uses vector bases (see Hanert et al., 2003, 2009).

4. Numerical examples

Initially, the model was applied to a test case for a freely propagating Kelvin wave in a circular basin (Ham et al., 2007). The basin is 250 km in radius, is 5 m in depth, has a constant latitude of 45° for the Coriolis term, and has an initial velocity and sea level specified. The linear shallow water equations are used where depth is constant in the continuity equation, and there are no friction or advection terms. The same grid as described in Ham et al. (2007) was used in this test with a time step of 20 min. The results are for the FE model using RT_0 elements unless stated otherwise.

For a semi-implicit treatment of the gravity wave terms and a forward Euler and AB2 treatment of the Coriolis terms, the solution is unstable. The addition of bottom friction leads to a stable solution where the wave decays over several rotations.

Using the modified form for AB2, the stability of the solution depends on the time weight θ. For $\theta = 0.5$, the solution becomes unstable. For $\theta \geqslant 0.505$, the solution remains stable.

Again using a semi-implicit treatment for the gravity wave terms but a AB3 treatment for the Coriolis term, the stability of the solution depends on the time weight θ. For $\theta = 0.5$, the solution becomes unstable after about 4 rotations of the wave. For $\theta = 0.502$, the solution slowly becomes unstable over approximately 5200 rotations. For $\theta \geqslant 0.503$, the solution remains stable over the entire simulation of 1200 days.

The finite element model used in all the tests except FBT utilizes an unstructured, staggered grid with the RT_0 element (Walters and Casulli, 1998; Walters, 2005). Since there is only one velocity degree of freedom on each edge, the FBT scheme cannot be applied. Hence a different finite element model which uses the $P_1^{NC} - P_1$ element was utilized (Hanert et al., 2005, 2009). This discretization has two velocity degrees of freedom (u,v) on each edge. Using this model, a stable solution was also obtained for the FBT scheme.

These results are in agreement with the analysis presented above. The forward Euler and AB2 approximations for the Coriolis term are unconditionally unstable in the absence of friction. A traditional formulation for bottom friction (3) stabilizes the solution, particularly for the shallow depth in this test case. The modified AB2 approximation is unstable for $\theta = 0.5$ but stable for a small increase ($\theta \approx .505$) For the AB3 approximation, the solution is unstable for $\theta = 0.5$ as indicated by Durran (1991) and shown in our analysis. For $\theta = 0.503$ the solution is stable. This is a slightly higher value than derived in the analysis and is probably due to the irregular grid used for this test case. The FBT scheme is stable for $\theta = 0.5$.

Next, we present numerical examples ranging from coastal circulation with considerable frictional effects to regional circulation where the outer boundaries are in deep water beyond the continental shelf. These examples are intended as a test of the results derived in the analysis when extended to the full nonlinear 2D and 3D SWE. We have chosen fE and AB3 to examine as these characterize the general response of the schemes we have examined. In particular, both these explicit methods should give reasonable results in a high-friction environment, but the forward Euler should be unstable in the larger domain. All these results were derived using the FE model with RT_0 elements.

4.1. Cook Strait model

Cook Strait lies between the North Island and the South Island of New Zealand. The semi-diurnal tides have a large phase difference across this area resulting in strong tidal currents (Walters et al., 2001). The computational domain and bathymetry used here are shown in Fig. 10. Note the relatively shallow shelf environment in the west, and the steep continental slope and deep ocean trench in the east.

The model is set up for three-dimensional circulation with tidal forcing at the open boundaries and wind stress at the surface. The tidal forcing was derived from a regional model (Walters et al., 2001), the Z0 component was derived from regional climatology (Rickard, personal communication), and the winds were taken from a site on Cape Farewell at the western end of the strait.

Initial calculations with only tides for forcing (no Z0) were stable for both explicit methods (fE and AB3). However using fE, the model became unstable near the northeast part of the open boundary when the Z0 component was added. The Z0 boundary data contains a loop of the East Auckland current which is essentially geostrophic and this is where the instability arises. On the other hand, the AB3 approach was stable.

These results can be interpreted in terms of the stability analysis. Both explicit methods are stable with sufficient frictional damping such as typically occurs in a coastal environment. The instability with fE occurs in deep water where frictional damping is small and for the zero frequency component of the tide. This follows from an examination of Fig. 3 (for fE) and 8 (for AB3).

For an accuracy assessment, the model was run for 30 days of simulated time followed by a harmonic analysis of the results. A

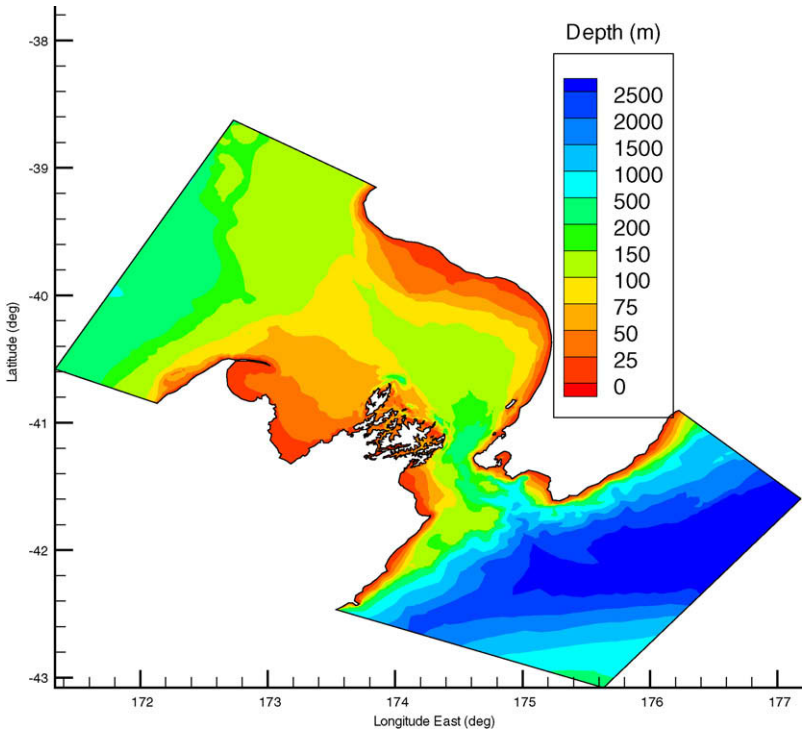

Fig. 10. Spatial domain and bathymetry for the Cook Strait grid.

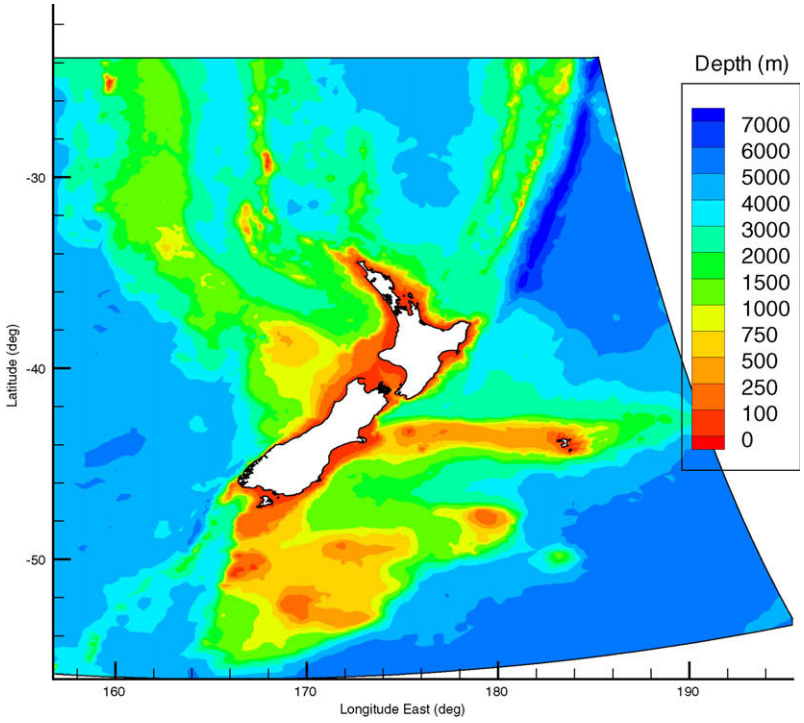

Fig. 11. Spatial domain and bathymetry for the NZLAM grid.

comparison with observations shows that the amplitude and phase errors in the tidal harmonics are typically a few cm. and a few degrees for the largest constituents.

4.2. New Zealand forecast model

A two-dimensional version of the model that calculates sea surface height (SSH) is part of a larger forecasting system for New Zealand collectively known as EcoConnect. The larger system is comprised of a local area weather model (New Zealand Local Area Model – NZLAM), a wave model (WaveWatch III), the SSH model described here (RiCOM), and a runoff model (Topnet). The SSH model is forced by surface pressure and winds from the weather model, and tides derived from a global tide model (Matsumoto et al., 1995). The spatial domain and bathymetry of the SSH model are shown in Fig. 11.

As opposed to the Cook Strait model, most of the spatial domain is in deep water seaward of the continental shelves. Maximum depth reaches 9000 m in the Tonga–Kermadec trench northeast of New Zealand. In the deep ocean, frictional dissipation is low which favors the AB3 explicit approach to discretizing the Coriolis term.

Initial calculations with fE approximation gave reasonable results for the initial period (a few days) but strong and unrealistic gyres eventually developed in deep water in the southeast part of the grid. These could be controlled but not eliminated with excessive damping (low-order interpolation with the semi-Lagrange advection scheme, large values for time weighting) but these results were not satisfactory.

On the other hand, calculations with AB3 approximation do not require additional damping and do not lead to instabilities or unrealistic gyres. Following this approach, we have run the model for 30 days of simulated time followed by a harmonic analysis of the results. An initial comparison with observations (Walters et al., 2001) shows typical amplitude errors of 3–5 cm for the M_2 and phase errors of 5–8° also for the M_2 which is the largest constituent. Amplitude and phase maps of the largest constituents are similar to those shown in (Walters et al., 2001).

5. Conclusions

Development of a coastal and ocean model has led to a semi-implicit time-integration scheme that removes restrictive stability constraints on gravity waves and vertical friction terms. However, the efficient integration of the Coriolis term requires special attention. When the numerical model uses a staggered grid with normal velocity degrees of freedom, implicit integration of this term is very inefficient as it leads to inversion of a large, sparse velocity matrix. For models that use full velocity vectors, efficiency may also be reduced because the matrix is no longer symmetric. On the other hand, published methods suggest that many if not most explicit methods to integrate the Coriolis term are unstable in this situation.

Here, an analysis of the discretized shallow water equations indicates that some of the explicit methods are stable or stable under somewhat relaxed conditions. The forward Euler and AB2 scheme are always unstable, but can be stabilized in shallow water environments (but not deep water) by bottom friction. However, (Marshall et al., 1997) indicate how the weights for AB2 can be modified in order to achieve stability but at lower-order accuracy. Our results indicate that a weak stability constraint is still present.

Of the schemes we examined, the third-order Adams–Bashforth and FBT schemes showed good behavior. AB3 has a minor stability constraint on θ, the time weight. This technique is particularly useful for staggered grid models such as ones with the RT_0 element which have one velocity degree of freedom (normal velocity) on each edge. Some existing models already use this technique (Shchepetkin and McWilliams, 2005). The AB3 has better accuracy than the other schemes. The FBT scheme introduces no additional stability constraints, but can only be used with models that use full velocity vectors (at least in the unstructured grid case) and hence is ideally suited to the $P_1^{NC} - P_1$ element.

Test simulations with a Kelvin wave in a circular basin verify these findings. Additional examples of coastal and deep ocean simulations are also in agreement with this analysis. These examples use the full non-linear SWE with measured bathymetry for coastal and regional scale simulations.

Acknowledgement

E.H. thanks the Nuffield Foundation for a newly appointed lecturer award.

References

Barragy, E., Walters, R.A., 1998. Parallel iterative solution for h and p approximations of the shallow water equations. Adv. Water Resour. 21 (5), 327–337.

Beckers, J., Deleersnijder, E., 1993. Stability of a FBTCS scheme applied to the propagation of shallow-water inertia-gravity waves on various space grids. J. Comput. Phys. 108, 95–104.

Casulli, V., Cattani, E., 1994. Stability, accuracy, and efficiency of a semi-implicit method for three-dimensional shallow water flow. Comput. Math. Applic. 27, 99–112.

Casulli, V., Walters, R.A., 2000. An unstructured grid, three-dimensional model based on the shallow water equations. Int. J. Numer. Meth. Fluids 32, 331–348.

Casulli, V., Zanolli, P., 2002. Semi-implicit numerical modeling of nonhydrostatic free-surface flows for environmental problems. Math. Comput. Model. 36, 1131–1149.

Danilov, S., Kivman, G., Schröter, J., 2004. A finite element ocean model: principles and evaluation. Ocean Modell. 6, 125–150.

Dukowicz, J.K., Smith, R.D., 1994. Implicit free-surface method for the Bryan–Cox–Semtner ocean model. J. Geophys. Res. 99 (C4), 7991–8014.

Durran, D.R., 1991. The third-order Adams–Bashforth method: an attractive alternative to Leapfrog time differencing. Mon. Weather Rev. 119, 702–720.

Fringer, O.B., Gerrirsen, M., Street, R.L., 2006. An unstructured grid, finite volume, nonhydrostatic, parallel coastal ocean simulator. Ocean Modell. 14, 139–173.

Ham, D.A., Kramer, S.C., Stelling, G.S., Pietrzak, J., 2007. The symmetry and stability of unstructured mesh C-grid shallow water models under the influence of Coriolis. Ocean Modell. 16, 47–60.

Hanert, E., Legat, V., Deleersnijder, E., 2003. A comparison of three finite elements to solve the linear shallow water equations. Ocean Modell. 5, 17–35.

Hanert, E., Le Roux, D.Y., Legat, V., Deleersnijder, E., 2005. An efficient Eulerian finite element method for the shallow water equations. Ocean Modell. 10, 115–136.

Hanert, E., Walters, R.A., Le Roux, D.Y, Pietrzak, J., 2009. A tale of two elements: $P_1^{NC} - P_1$ and RT_0. Ocean Modell. 28, 24–33.

Kanarska, Y., Shchepetkin, A., McWilliams, J.C., 2007. Algorithm for non-hydrostatic dynamics in the regional ocean modeling system. Ocean Modell. 18, 143–174.

Kwok, Y.-K., 1996. Accuracy and stability analysis of numerical schemes for the shallow water model. Numer. Meth. Part. D. E. 12, 85–98.

LeRoux, D.Y., Rostand, V., Pouliot, B., 2007. Analysis of numerically-induced oscillations in 2D finite-element shallow-water models, Part I: inertia-gravity waves. SIAM J. Sci. Comp. 29, 331–360.

Leendertse, J.J, 1967. Aspects of a computational model for long period water wave propagation. Tech Report RM-5294-PR, Santa Monica, Rand Memorandum.

Marshall, J., Adcroft, A., Hill, C., Perelman, L., Heisy, C., 1997. A finite-volume, incompressible Navier–Stokes model for studies of the ocean on parallel computers. J. Geophys. Res. 102 (C3), 5753–5766.

Matsumoto, K., Ooe, M., Sato, T., Segawa, J., 1995. Ocean tide model obtained from TOPEX/POSEIDON altimetry data. J. Geophys. Res. 100 (C12), 25,319–25,330.

Mesinger, F., Arakawa, A., 1976. Numerical Methods Used in Atmospheric Models, vol. 1, GARP Publ. Ser. 17, World Meteorological Organization, 64 pp.

Pinder, G.F., Gray, W.G., 1977. Finite elements in surface and subsurface hydrology. Academic Press.

Shchepetkin, A., McWilliams, J.C., 2005. The regional ocean modeling system: a split–explicit, free-surface, topography-following-coordinate oceanic model. Ocean Modell. 9, 347–404.

Sielecki, A., 1968. An energy conserving difference scheme for the storm surge equations. Mon. Weather Rev. 96, 150–156.

Walters, R.A., 2005. A semi-implicit finite element model for non-hydrostatic (dispersive) surface waves. Int. J. Numer. Meth. Fluids 49, 721–737.

Walters, R.A., Casulli, V., 1998. A robust, finite element model for hydrostatic surface water flows. Comm. Numer. Meth. Eng. 14, 931–940.

Walters, R.A., Goring, D.G., Bell, R.G., 2001. Ocean tides around New Zealand. New Zeal. J. Mar. Fresh. Res. 35, 567–579.

Zhang, Y., Baptista, A.M., 2008. SELFE: a semi-implicit Eulerian–Lagrangian finite-element model for cross-scale ocean circulation. Ocean Modell. 21, 71–96.